

Study of the magnetostructural transition in critical-element free $\text{Mn}_{1-x}\text{Ni}_{1-x}\text{Fe}_{2x}\text{Si}_{0.95}\text{Al}_{0.05}$

Cite as: AIP Advances **13**, 025215 (2023); <https://doi.org/10.1063/9.0000511>

Submitted: 03 October 2022 • Accepted: 25 November 2022 • Published Online: 03 February 2023

 Bruno G. F. Eggert,  Kun Wang,  Sina Jafarzadeh, et al.

COLLECTIONS

Paper published as part of the special topic on [67th Annual Conference on Magnetism and Magnetic Materials](#)



View Online



Export Citation



CrossMark

ARTICLES YOU MAY BE INTERESTED IN

[Structural, magnetic, and magnetocaloric characterization of NiMnSn microwires prepared by Taylor-Ulitovsky technique](#)

AIP Advances **13**, 025101 (2023); <https://doi.org/10.1063/9.0000549>

[Influence of the particle size on a MnFe\(P,Si,B\) compound with giant magnetocaloric effect](#)

AIP Advances **13**, 025203 (2023); <https://doi.org/10.1063/9.0000371>

[Current perspective in magnetocaloric materials research](#)

Journal of Applied Physics **133**, 040903 (2023); <https://doi.org/10.1063/5.0130035>



Study of the magnetostructural transition in critical-element free $\text{Mn}_{1-x}\text{Ni}_{1-x}\text{Fe}_{2x}\text{Si}_{0.95}\text{Al}_{0.05}$

Cite as: AIP Advances 13, 025215 (2023); doi: 10.1063/9.0000511

Submitted: 3 October 2022 • Accepted: 25 November 2022 •

Published Online: 3 February 2023






View Online



Export Citation



CrossMark

Bruno G. F. Eggert,¹  Kun Wang,²  Sina Jafarzadeh,²  Christian R. Bahl,²  Bjørn C. Hauback,¹  and Christoph Frommen^{1,a)} 

AFFILIATIONS

¹Department for Hydrogen Technology, Institute for Energy Technology (IFE), P.O. Box 40, NO-2027 Kjeller, Norway

²Department of Energy Conversion and Storage, Technical University of Denmark (DTU), Anker Engeldunds Vej B301, DK-2800 Kgs. Lyngby, Denmark

Note: This paper was presented at the 67th Annual Conference on Magnetism and Magnetic Materials.

^{a)}Author to whom correspondence should be addressed: Christoph.frommen@ife.no

ABSTRACT

Two different heat treatments have been carried out on similar $\text{Mn}_{1-x}\text{Ni}_{1-x}\text{Fe}_{2x}\text{Si}_{0.95}\text{Al}_{0.05}$ compositions with magnetostructural transitions between hexagonal and orthorhombic crystal structures around room temperature. The samples were analyzed concerning their structural, microstructural, magnetic, and caloric properties. The results show that the introduction of a high-temperature step, before the heat treatment (1073 K/7 days) usually used in the literature for such compounds modifies the microstructure, leading to sharper transitions with shorter transition widths, and stronger latent heat peaks. Magnetic field-assisted calorimetry and vibrating sample magnetometry provide methods to assess the effect of magnetic field on the broad transitions for the sample with $x = 0.32$ and the sharp transitions seen in the sample with $x = 0.31$.

© 2023 Author(s). All article content, except where otherwise noted, is licensed under a Creative Commons Attribution (CC BY) license (<http://creativecommons.org/licenses/by/4.0/>). <https://doi.org/10.1063/9.0000511>

INTRODUCTION

To fully realize solid-state cooling by magnetic refrigeration, further understanding of the impact of microstructure on the magnetocaloric effect is required. Modification of the microstructure can influence transition kinetics, leading to stronger, more efficient transformations, while lowering hysteresis.¹ Besides microstructure, new compositions that modify the intrinsic aspects of transitions and allow for higher reversibility also need to be explored.

In this context, the $\text{MM}'\text{X}$ compounds (where M and M' are transition metals and X is a p-block element) are promising candidates for use with room temperature (RT) magnetic heat conversion technologies.^{2–5} This is due to their versatile martensitic (diffusionless) transitions between a ferromagnetic martensite orthorhombic (TiNiSi structure-type, space group: Pnma) crystal structure and a paramagnetic austenite with a hexagonal structure (Ni_2In structure-type, space group: $\text{P6}_3/\text{mmc}$). This can lead to a strong isothermal entropy change (ΔS_m) and reasonable adiabatic temperature change (ΔT_{ad}). Such magnetostructural transitions (MSTs) are only possible

by substituting one or more elements from the parent $\text{MM}'\text{X}$ compound, which in turn modifies the structural transition temperature (T_{str}) and Curie Temperature (T_C) of both structures, making them coincide.

Recently, modifications of the (2a) Mn site by Fe and (2c) Si site by Al (when referring to the hexagonal crystal structure) successfully induced T_{str} towards RT.^{2,4,6} Similarly, (2d) Ni site substitution by Fe has also been discussed.⁷ In previous reports, $\text{MM}'\text{X}$ materials have been produced by arc melting succeeded by thermal treatment at temperatures around 1073 K (800 °C) for an extended period of time (4–7 days), followed by quenching to RT.^{2,4,8,9} However, little attention has been given to alternative heat treatment procedures for this kind of materials.

In this article, we report on the properties of two $\text{Mn}_{1-x}\text{Ni}_{1-x}\text{Fe}_{2x}\text{Si}_{0.95}\text{Al}_{0.05}$ compounds synthesized by arc melting which are heat treated by two different methods: with a single 1073 K step for 168 hours (sample A), and a 1073 K step for 168 hours preceded by a high temperature step at 1323 K for 5 hours (sample B), being quenched in water afterwards. Further

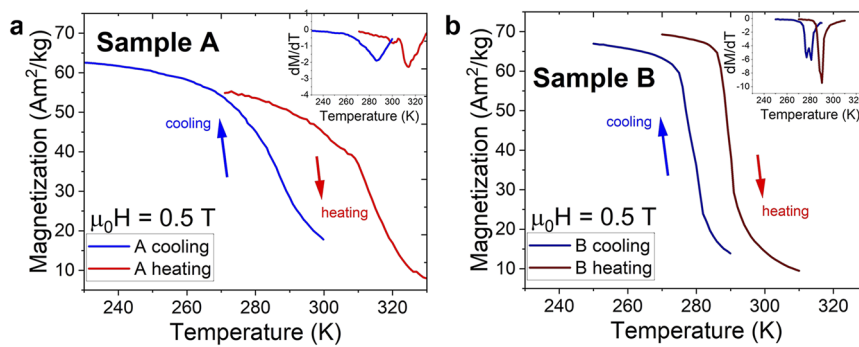


FIG. 1. Temperature-dependent magnetization for sample A and B evidencing the change in the magnetic transition due to the two different heat treatment procedures.

description of experimental and characterization methods is given in the supplementary information.

RESULTS

The magnetic transitions with an applied field of 0.5 T are presented in the temperature-dependent curves in Fig. 1. They are characterized by a decrease (or increase) of the magnetization during heating (or cooling) of the ingots. Transition values obtained from VSM are summarized in Table S1 in the [supplementary material](#). The T_{str} value is determined from the derivative of the magnetization. The transitions in sample A (Fig. 1(a)) are broad and occur at 314 and 286 K during heating and cooling, respectively. The magnetization values during heating are changing from 55 to 8 Am²/kg ($\Delta M = 47$ Am²/kg) in a temperature range of 57 K, from 272 to 329 K. The hysteresis values are also very high, reaching up to 27 K between the two transformations. In sample B, the transitions occur

at 290 and 278 K during heating and cooling respectively, and are sharper, as indicated by the higher derivative of magnetization with temperature, seen in the inset of Fig. 1(b). The hysteresis values for sample B are also smaller than for sample A, reaching up to 11.3 K. An interesting feature of the cooling curve is the presence of two derivatives, indicating two different values for T_{str} . During the heating procedure, the magnetization in sample B changes from 66 to 17 Am²/kg ($\Delta M = 49$ Am²/kg) in a temperature interval of 15 K, between 282 and 297 K. Therefore, the shifts in magnetization occur within smaller temperature spans in sample B, compared to sample A. To understand the difference between the transitions for the two samples, Powder X-ray Diffraction was carried out at RT, and is referred to in the [supplementary material](#). The results indicate very similar phase contents between sample A and B. The way that such phases are distributed along the microstructure could shed light on its magnetic behavior. Therefore, optical microscopy and SEM measurements were performed.

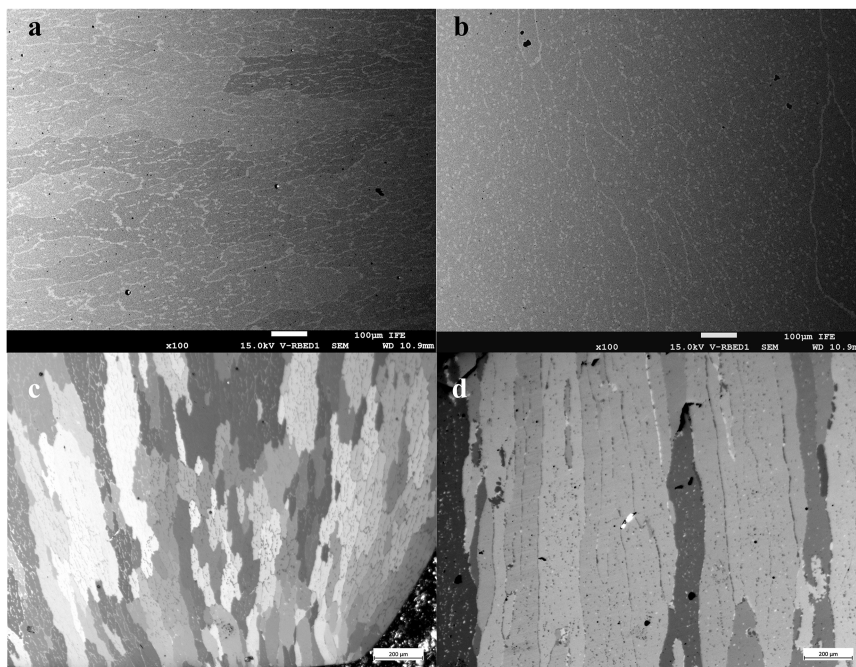


FIG. 2. Back-scattered SEM micrographs for (a) sample A and (b) sample B with 100 times magnification. Polarized optical microscopy images in (c) sample A and (d) sample B with 31.5 x magnification.

TABLE I. Chemical composition of $\text{Mn}_{1-x}\text{Ni}_{1-x}\text{Fe}_{2x}\text{Si}_{0.95}\text{Al}_{0.05}$ with $x = 0.32$ (sample A) and 0.31 (sample B) as measured by EDS.

Sample	Nominal composition of the alloy (formula units)	Area comp. (formula units)	Main phase composition (formula units)	Sample	Nominal composition of the alloy (formula units)	Area comp. (formula units)	Main phase composition (formula units)
A				B			
Mn(1 - x)	0.68	0.69 ± 0.01	0.67 ± 0.01	Mn(1 - x)	0.69	0.72 ± 0.01	0.69 ± 0.01
Ni(1 - x)	0.68	0.69 ± 0.01	0.66 ± 0.01	Ni(1 - x)	0.69	0.68 ± 0.01	0.64 ± 0.01
Fe(2x)	0.64 (x = 0.32)	0.64 ± 0.01	0.68 ± 0.01	Fe(2x)	0.62 (x = 0.31)	0.61 ± 0.01	0.66 ± 0.01
Si(0.95)	0.95	0.93 ± 0.01	0.94 ± 0.01	Si(0.95)	0.95	0.94 ± 0.01	0.95 ± 0.01
Al(0.05)	0.05	0.05 ± 0.01	0.05 ± 0.01	Al(0.05)	0.05	0.05 ± 0.01	0.06 ± 0.01

Back-scattered SEM micrographs for samples A and B are shown in Fig. 2. The ingots were prepared to display the solidification front of the alloys, i.e., the cross-section parallel to the arc direction during the arc melting process. For sample A (Fig. 2(a)) two phases can be seen from the contrast in the images, which correspond to the $\text{Ni}_2\text{In}/\text{TiNiSi}$ (dark areas, the main phase) and MgZn_2 hexagonal (clear areas) phases, respectively. Additionally, the secondary MgZn_2 hexagonal phase can be seen inside the grains in different morphologies: as lines in sample A, and as lines and rounded precipitates in sample B (seen in Fig 2(b)).

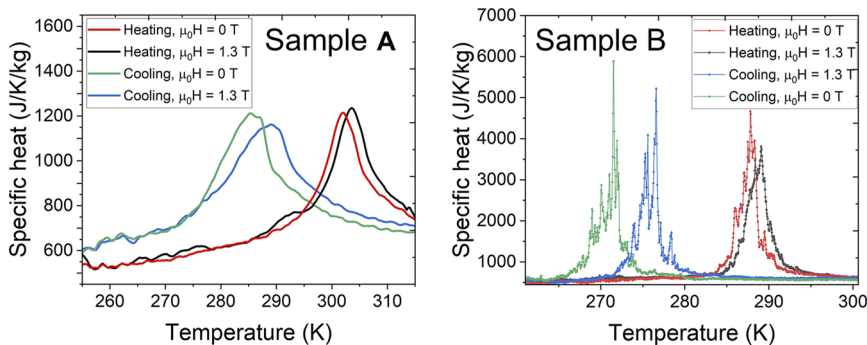
The average composition for sample A and B as determined by area EDS measurements is similar to the nominal composition (see Table I). Regarding the area composition of the main phase (Ni_2In hexagonal/ TiNiSi orthorhombic structure-type), the results display some differences from nominal compositions regarding the Ni content, which is slightly smaller than the nominal alloy composition. This can be correlated to the effect of different heat treatments, which might induce different phase fractions. The composition of the hexagonal Ni_2In phase is correlated to T_{str} , where higher modifications of the parent compound (Fe and Al modification) bring T_{str} to lower values. Between Fe and Al, Al has a stronger influence on the modification of T_{str} , which could explain the slightly lower T_{str} observed in sample B.

Due to the large grain sizes, the effect of the two different heat treatments can be better understood under lower magnifications in polarized light microscopy, see Figs. 2(c) and 2(d). The microstructure yielding from the regular heat treatment process is shown in Fig. 2(c), with columnar long grains yielding from the arc melting process. Different grey hues seen in the image represent different

orientations in the grains, making it possible to estimate the grain sizes. The grain sizes feature great dispersion, ranging in length from tens of microns to several hundred microns.

The additional high-temperature step for sample B modifies the microstructure, as seen in Fig. 2(d). The grains have smaller variations in their crystallographic orientations, which leads to a smaller grey hue variation. Furthermore, the grains are larger compared to sample A, but with smaller size dispersion. Therefore, the higher temperature step of 5 hours at 1323 K creates substantial grain growth before the 168 hour (1 week) step. With bigger grains, a smaller amount of grain boundary areas is present in sample B compared to sample A. To further the understanding of the differences between the two samples, the transitions were analyzed with in-field DSC experiments.

Two ingots were selected, with masses of 6.41 and 4.41 mg for sample A and B, respectively. These small masses were chosen in order to minimize the risk of sample movement due to the applied field. A comparison of the transitions observed in both samples with a heating rate of 1 K/min is shown in Fig. 3, for applied fields of 0 and 1.3 T. The T_{str} and the hysteresis values for both samples are displayed in Table S1. It is possible to observe larger transition widths during cooling transformations than on heating for both samples. A broad transition spanning between 25–30 K is observed for sample A, with the cooling transformation temperature ($T_{\text{str-h-o}}$) occurring at 287.8 K. The heating transformation temperature ($T_{\text{str-o-h}}$) occurs at 302.0 K. Sample B features a sharper transition, with a width of 7–10 K occurring at $T_{\text{str-h-o}}$ of 271.5 upon cooling and $T_{\text{str-o-h}}$ of 287.8 K during heating. The absolute latent heat peak associated with the transitions in sample A is between

**FIG. 3.** Specific heat curves for sample A and B obtained from in-field DSC with applied fields of $\mu_0H = 0$ and 1.3 T.

600–700 J/K⁻¹kg⁻¹, compared to 4000–5000 J/K.kg in sample B, which is a remarkable difference. Both samples appear to display a large thermal hysteresis of around 16 K between heating and cooling transformations.

A shift of peak positions to higher temperatures as the magnetic field is increased occurs for both transitions, with smaller shifts occurring during the heating transformation than compared to the cooling, for both samples. In both samples, the shift of $T_{\text{str}_{o-h}}$ is around 1 K/T, whereas $T_{\text{str}_{h-o}}$ is 2.9 and 3.9 K/T for samples A and B, respectively. This leads to smaller hysteresis values with higher applied fields.

DISCUSSION

The transformations during cooling and heating need to be analyzed separately. During heating transformation (ortho-to-hex), an anisotropic contraction occurs, with the compression along the *a* direction and an expansion in the *c* direction (based on the hexagonal unit cell).¹⁰ This leads to an overall compression of the lattice, which induces a residual tensile stress. This residual stress impacts the material in addition to the expansion of the lattice during the hexagonal to orthorhombic (cooling) transformation, creating new surface area (cracking) to accommodate for the stresses in the brittle material. After several cycles, this will lower the cohesion between the particles, eventually pulverizing them, lowering the reversibility. However, some recent studies show promising results employing ductile metal composites that can keep cohesion of the particles and accommodate for the transformation stresses appropriately.¹¹

Regarding the larger width of cooling transformations compared to heating, the release of residual tensile stress during the cooling transformation could contribute to lower the nucleation threshold of the orthorhombic phase, thus acting differently on the transitions during cooling than during heating. With a lower nucleation threshold for the martensitic phase, each grain would transition more easily, thereby spreading the transformation during cooling.

The sharp peaks in the specific heat curves for sample B (Fig. 3 and S3) can be associated to more homogeneous (lower) dispersion of the elements in the lattice (at the local level, not easily detectable by regular EDS techniques), since Mn, Ni and Fe can interchangeably occupy *2a* and *2d* sites in the *Ni₂In* crystal structure. This would lower the dispersion of the T_{str} values. A second reason is the increase of average grain sizes and decrease of its dispersion, which could modify the growth of new orth./hex. phases. As the mechanism of the growth of martensitic phase fronts is only deterred by interphase and grain boundaries, it would lead to a smaller volume of inhibiting agents during the transformation of sample B (with decreased volume of grain boundary areas) compared to sample A, and therefore easily transforming bigger volumes at once.

A more homogeneous structure and bigger grain sizes results in higher latent heat spikes (up to 5000 J/K⁻¹kg⁻¹), higher magnetization derivatives, and sharper transitions widths (7–10 K) for sample B. In comparison, the transitions measured by DSC for sample A span between 20–25 K, with a much smaller latent heat peak. While the transition appears broader, it is of first order, as a large thermal hysteresis is observed. A supporting evidence for the effect of grain size on the transition width is that in other MM'X system, (Mn,Fe)Ni(SiAl), melt-spun ribbons with small grain size in range of

10 microns feature much wider transition width, and subsequently, lower ΔS_m than arc-melted/bulk (Mn,Fe)Ni(Si,Al) samples undergoing long heat-treatment steps with large grain sizes.^{5,9} Another method to compare both samples could be by analyzing the structural transition by temperature-dependent PXD. As the sample is typically grinded to submicrometric particles, they are not susceptible to the influence of different grain sizes, allowing each particle to transition on its own. If a sample features better homogeneity, all particles will transition within a smaller transition width.

CONCLUSION

The MST of $\text{Mn}_{1-x}\text{Ni}_{1-x}\text{Fe}_{2x}\text{Si}_{0.95}\text{Al}_{0.05}$ alloys was studied as a function of two different heat treatment procedures. The conventional heat treatment plateau at 1073 K (sample A) has been compared to a heat treatment where a high temperature step (1323 K) is introduced right before the regular heat treatment plateau, also at 1073 K (sample B). Temperature-dependent magnetization results reveal that sample A features a broad magnetization change across RT, with transitions occurring between 314 to 286 K, for heating and cooling transformations, while sample B features a sharper magnetization variation, occurring at 290 and 280 K for heating and cooling, respectively.

Despite similar phase presences, average structures and compositions as measured by PXD and SEM/EDS, much larger grains are observed for sample B than for sample A. The results indicate that the high temperature step induced better homogeneity and increased grain sizes, which would induce higher volume fractions to transform at once, leading to increased latent heat spikes. Nevertheless, a more detailed study on the isothermal entropy changes of heating and cooling transitions is required to obtain a full picture of the effect of heat treatment on the properties of $\text{Mn}_{1-x}\text{Ni}_{1-x}\text{Fe}_{2x}\text{Si}_{0.95}\text{Al}_{0.05}$ compounds.

SUPPLEMENTARY MATERIAL

See [supplementary material](#) for the description of experimental methods and further data analysis.

ACKNOWLEDGMENTS

This work was financed by The Research Council of Norway through the NANO2021 program, Project No. 287150.

AUTHOR DECLARATIONS

Conflict of Interest

The authors have no conflicts to disclose.

Author Contributions

Bruno G. F. Eggert: Conceptualization (equal); Data curation (equal); Formal analysis (equal); Investigation (equal); Methodology (equal); Visualization (equal); Writing – original draft (equal); Writing – review & editing (equal). **Kun Wang:** Investigation (equal); Resources (equal); Writing – review & editing (equal). **Sina Jafarzadeh:** Investigation (equal); Resources (equal). **Christian R. Bahl:** Investigation (equal); Resources (equal); Writing – review &

editing (equal). **Bjørn C. Hauback**: Supervision (equal); Writing – review & editing (equal). **Christoph Frommen**: Funding acquisition (equal); Project administration (equal); Supervision (equal); Writing – review & editing (equal).

DATA AVAILABILITY

The data that support the findings of this study are available from the corresponding author upon reasonable request.

REFERENCES

- ¹O. Gutfleisch, T. Gottschall, M. Fries, D. Benke, I. Radulov, K. P. Skokov, H. Wende, M. Gruner, M. Acet, P. Entel, and M. Farle, *Philos. Trans. R. Soc. A Math. Phys. Eng. Sci.* **374**, 6607 (2016).
- ²A. Biswas, N. A. Zarkevich, Y. Mudryk, A. K. Pathak, A. V. Smirnov, V. P. Balema, D. D. Johnson, and V. K. Pecharsky, *J. Appl. Phys.* **129**, 193901 (2021).
- ³S. K. Pal, C. Frommen, S. Kumar, B. C. Hauback, H. Fjellvåg, and G. Helgesen, *Mater. Des.* **195**, 109036 (2020).
- ⁴C. L. Zhang, H. F. Shi, Y. G. Nie, E. J. Ye, Z. D. Han, and D. H. Wang, *Appl. Phys. Lett.* **105**, 242403 (2014).
- ⁵L. M. Moreno-Ramírez, Á. Díaz-García, J. Y. Law, A. K. Giri, and V. Franco, *Intermetallics* **131**, 107083 (2021).
- ⁶M. L. Arreguín-Hernández, C. F. Sánchez-Valdés, and J. L. Sánchez Llamazares, *J. Magn. Magn. Mater.* **533**, 168021 (2021).
- ⁷B. Nuendute, W. Hanggai, H. Yibole, B. Tana, O. Tegus, and F. Guillou, *Crystals* **12**, 233 (2022).
- ⁸C. L. Zhang, Y. G. Nie, H. F. Shi, E. J. Ye, J. Q. Zhao, Z. D. Han, H. C. Xuan, and D. H. Wang, *J. Magn. Magn. Mater.* **432**, 527 (2017).
- ⁹A. Biswas, A. K. Pathak, N. A. Zarkevich, X. Liu, Y. Mudryk, V. Balema, D. D. Johnson, and V. K. Pecharsky, *Acta Mater.* **180**, 341 (2019).
- ¹⁰T. Zhang, Y. Gong, B. Wang, D. Cen, and F. Xu, *J. Mater. Sci. Technol.* **104**, 59 (2022).
- ¹¹H. Zhou, K. Tao, B. Chen, H. Chen, K. Qiao, Z. Yu, J. Cong, R. Huang, S. V. Taskaev, and H. Zhang, *Acta Mater.* **229**, 117830 (2022).